J Therm Spray Tech (2023) 32:2603–2619
https://doi.org/10.1007/s11666-023-01662-7

ORIGINAL RESEARCH ARTICLE

Effect of Laser-Glazed Treatment on Thermal Cyclic Behavior of Plasma-Sprayed Lanthanum Zirconate/Yttria-Stabilized Zirconia Double Ceramic Layered on NiCoCrAlYTa-coated Inconel

Azrina Arshad[1,2] · Muhamad Azizi Mat Yajid[1] · Mohammadreza Daroonparvar[3] · Mohd Hasbullah Idris[1] · Intan Syaqirah Mohd Zulkifli[4] · Ahmed G. Hassan[1,5] · Zulhelmi Alif Abdul Halim[1]

Submitted: 19 March 2023 / in revised form: 11 September 2023 / Accepted: 13 September 2023 / Published online: 2 October 2023

Abstract This paper investigates the thermal barrier coating (TBC) performance of $La_2Zr_2O_7$/ZrO (2-8 wt.%) Y_2O_3 coatings (LZ/YSZ TBCs) deposited using atmospheric plasma spray (APS) over high velocity oxy-fuel (HVOF) NiCoCrAlYTa coated on Inconel 625. On the outermost surface of the double-layered coating, a laser glazing method was used to treat the TBC systems. Specifically, a Nd:YAG pulsed laser was used to change the surface layer of plasma-sprayed $La_2Zr_2O_7$ top coatings. The study found that the laser glazing treatment resulted in a higher number of temperature cycles needed to generate 5-20% spallation of the top surface of coatings, with 100 cycles compared to 30 cycles in the as-sprayed coatings. This improvement in performance was attributed to the dense surface of the laser-glazed LZ topcoat, which led to a lower thermally grown oxide (TGO) layer growth rate and improved TBC lifetime. Furthermore, the strain adaptation through segmented cracks that were created by laser glazing may have contributed to the enhanced TBC performance.

Keywords coating materials · laser processing · microstructure · thermal barrier coating · thermal cyclic · thermally grown oxide layer

✉ Azrina Arshad
azrinaa@unikl.edu.my

✉ Muhamad Azizi Mat Yajid
azizi_my@mail.fkm.utm.my

✉ Mohammadreza Daroonparvar
mr.daroonparvar@yahoo.com

[1] Faculty of Mechanical Engineering, Universiti Teknologi Malaysia, 81310 Johor Bahru, Johor, Malaysia

[2] Quality Engineering Section, Malaysian Institute of Industrial Technology, Universiti Kuala Lumpur, 81750 Johor Bahru, Johor, Malaysia

[3] Department of Mechanical Engineering, University of Nevada Reno, Reno, NV 89557, USA

[4] INTI International University, Persiaran Perdana BBN, Putra Nilai, 71800 Nilai, Negeri Sembilan, Malaysia

[5] Faculty of Engineering, University of Thi-Qar, Thi-Qar, Iraq

Introduction

Higher operating temperatures are required for advanced gas turbine engines to achieve greater thermal efficiencies and durability. In the early development of gas turbines, the inlet temperature was approximately 550 °C for Neuchatel gas turbine in Switzerland in 1939 (Ref 1). After tremendous advances by gas engine manufacturers, modern gas turbine engines have significantly increased the gas inlet temperature up to 1380 °C (Ref 2). Thermal barrier coatings (TBCs) have been widely used as thermal insulation on the surfaces of engine components such as vanes and blades to extend service life at high operating temperatures (Ref 3-5). The main function of the TBC is to reduce the temperature of metallic components, which aids in improving oxidation and corrosion resistance and so increases their durability (Ref 6, 7). Aside from the metallic substrate, TBC systems have two distinct layers: MCrAlY as a bond coat, with M being Co, Ni, or both, and a ceramic top coat (Ref 8). The application of NiCoCrAlYTa as a bond coat is relatively recent, and it has aided in significantly improving oxide scale adhesion and slowing the rapid diffusion of Al (Ref 9, 10). The addition of alloying elements like Co and Ta can increase the diffusion barrier's capability as well as its superior resistance to corrosion (Ref 11). The conventional ceramic top coat

material consists of 6-8 wt.% Y_2O_3-stabilized zirconia (YSZ) (Ref 12). However, a mismatch in the thermal expansion coefficients of the ceramic topcoat and the metallic bond coatings accelerates the sintering phase transformation above 1200 °C, limiting the service life of YSZ for long-term operation (Ref 13-15). Lanthanum zirconate ($La_2Zr_2O_7$) with a pyrochlore structure has been described as a newly developed ceramic material for thermal barrier coating systems used in advanced gas turbines (Ref 16, 17) in order to increase the durability and performance of gas turbines as well as address the disadvantages of YSZ. Because of its high melting point, very low thermal conductivity, and reasonably high thermal stability up to 2000 °C (Ref 18), $La_2Zr_2O_7$ is a promising choice for high-temperature TBC applications.

TBC system failure is typically caused by spallation of the topcoat near the ceramic/TGO interface or within the ceramic topcoat, and it is also attributed to excessive growth of the thermally grown oxide (TGO) layer during oxidation (Ref 19, 20). The formation of TGO scale occurs when the metallic bond coat oxidizes at elevated temperatures (Ref 21). TGO formation that is dense, thinner, and continuous (with a slow growth rate) may act as a diffusion barrier to bond coat oxidation (Ref 22). Thicker TGO (with a high growth rate) might induce micro-cracks at the TGO/TC (topcoat) interface and expedite the formation of spinels on the Al_2O_3 layer during high temperature operation, finally leading to spallation to TBC. Evans A.G et al. (Ref 23) discovered that TBC failure occurs when the TGO reaches a critical thickness of 3-10 μm (Ref 24). Moreover, TBCs have a tendency to spall in cyclic high temperature conditions (Ref 25). Another aspect influencing TBC performance is the development of non-alumina oxides such as Cr_2O_3, NiO, and $Ni(Al,Cr)_2O_4$ spinels during high temperature oxidation, which causes tensile stress and accelerates the defect region in ceramic coatings (Ref 26). The crack generated by the development and rapid growth of TGO compromised the TBCs structure, providing more channels for oxygen diffusion (mainly via gas permeation mechanism) (Ref 27) and accelerating bond coat degradation during high temperature oxidation.

As a result, considerable experimental studies have been conducted to investigate the cause of TBC failure due to bond-coat oxidation, such as TGO layer growth (Ref 26, 28, 29) and phase transformation (Ref 30-32). Several researchers have focused on strategies for extending the lifetime of TBCs by modifying the chemical composition of TBC systems. To increase phase stability in the temperature range for TBCs applications, the chemical composition of ceramic top coats is altered by adding certain elements such as La (Ref 33-35), Sm (Ref 32), Gd (Ref 36). Zhou et al. (Ref 37) investigated some other rare earth-doped lanthanum zirconate-based ceramics. When compared to the YSZ coating, all of the doping rare earth cations significantly reduced thermal conductivity while increasing melting point and phase stability (Ref 36).

On the other hand, researchers have been exploring the use of a multilayer approach to modify the ceramic topcoat and effectively reduce oxygen diffusion toward the metallic bond coat. For instance, Daroonparvar et al. (Ref 12) added nano-alumina as a third layer on top of YSZ coating, while Nejati et al. (Ref 38) applied nano-Al_2O_3 to a ceria-stabilized zirconia (CSZ) coating. More recently, An et al. (Ref 27) sprayed YAG (Yttrium Aluminum Garnet) onto the top of coating. Another technique that has been investigated for improving the lifetime of thermal barrier coatings, especially during thermal cycles, is the use of a double-ceramic-layer thermal barrier coating (DCL-TBC) consisting of a top ceramic layer (TC1) and an interior ceramic layer (TC2). Wang et al. (Ref 39) and Zhou et al. (Ref 31) have both conducted research on this approach.

Laser glazing, or surface modification by laser, is an advanced processing technology that appears to be the most recent advancement in modifying the surface of thermal barrier coatings. This method has the potential to effectively reduce surface defects caused by plasma spraying, such as porosities. The pores, microcracks, and lamellar structure that are typical of plasma-sprayed ceramic coatings may facilitate the penetration of corrosive salts into the coating. As a result, there is interest in creating a denser layer to heal and densify the coatings through the post-treatment process. Previous research has shown that surface modification techniques such as laser glazing can reduce surface roughness and eliminate porosity to densify the top layer ceramic coatings structure and improve thermal shock resistance of the TBC by generating a controlled segmented crack network perpendicular to the surface (Ref 28-31). The porosity and surface morphology of the TBC can have a significant impact on its ability to protect the gas turbine components. Segmented cracks were claimed to be beneficial for accommodating the oxidation stress and mismatch stress during thermal cyclic testing (Ref 40, 41).

At present, extensive research has been carried out concerning laser glazing for plasma-sprayed YSZ coatings. Recently, there has been a surge of interest in applying laser glazing to different TBC materials, such as CYSZ, nanostructured YSZ, and GZ ceramic coatings. Most prior studies have focused on the impact of laser glazing on single-layer TBCs when exposed to conditions like hot corrosion and thermal shock. However, this paper claims novelty regarding laser surface modification for plasma-sprayed double-ceramic-layer LZ/YSZ TBCs. Its objective

is to comprehend the influence of the laser glazing process on the visual and microstructural aspects of these coatings. Specifically, it seeks to analyze the behavior of the LZ-DCL TBC system under cyclic oxidation conditions at elevated temperatures. To achieve this, a pulsed Nd:YAG laser was employed to modify the LZ topcoat on a conventional YSZ coating. Subsequently, thermal cyclic tests at 1000 °C were administered to both the as-sprayed and as-glazed TBC coatings within a high-purity argon-controlled environment.

Experimental Procedure

Samples Preparation and Coating Deposition

The substrate used for this study was Ni-based superalloy samples, with dimensions of 15 × 15 × 6 mm^3. The thermal barrier coating employed a double ceramic layer structure consisting of LZ as the top coat and an intermediate ceramic coating of 8YSZ on the metallic NiCoCrAlYTa bond coat (Metco AMDRY 997). The ceramic top coats utilized in the study were commercially available $La_2Zr_2O_7$ powder (Trans-Tech, Inc. Adamstown, MD, USA) and 8 wt.% yttria stabilized zirconia (ZrO_2-8 wt.% Y_2O_3, Metco 204 NS-G) powders, manufactured by Oerlikon Metco's. Table 1 provides information on the geometrical properties of the powder materials used in the samples, as well as the thickness of each layer.

In order to enhance the surface area, activate the surface, and improve the adhesion between the sprayed coating and substrate, the substrates underwent a process of grit blasting using alumina particles with a mesh size of 24-50 prior to the thermal spraying procedure. The utilization of the grit blasting technique resulted in a notable enhancement of the surface roughness of the substrate, as indicated by an increase in the Ra value to a range of 6-8 μm. After the grit blasting process, the substrates underwent a cleaning procedure using acetone in an ultrasonic bath for a duration of 15 minutes. This step was performed to eliminate any remaining contaminants on the substrates. In order to mitigate residual stresses in the coating during the process of thermal spraying, the specimens underwent a washing procedure followed by preheating at temperatures ranging from 70 to 100 °C prior to the application of the coating.

Coatings Deposition

NiCoCrAlYTa was deposited using the high velocity oxy fuel (HVOF) (Diamond Jet spray gun, DJ2600, Sulzer Metco, Switzerland) system as the bond coat on the Inconel 625 substrate. The HVOF spray process parameters are listed in Table 2, based on prior research (Ref 10). The top coats 8YSZ and LZ were deposited using an atmospheric plasma spray (APS) equipped with a 3 MB gun (Sulzer Metco, Switzerland). Table 3 also lists the spray process parameters used for coating using APS as originated from previous study (Ref 12) and (Ref 42), respectively. Previous researchers have optimized these parameters in terms of current, powder feed rate, and spray distance that resulted in good coating structure.

Laser Glazing on Plasma-Sprayed $La_2Zr_2O_7$ (LZ) Top Layer

After spraying process, LZ topcoat was post-plasma spray treated by a Nd:YAG pulsed laser (Q-Smart 850, Quantel model, manufactured by Lumibird, France) with a characteristic wavelength of 1064 nm, a pulse duration of 6-ns and a 10 Hz repetition rate. The focal length was 50 mm with spot diameter was 0.80 mm was chosen as the lens of laser. The laser beam distance was kept constant at 4 mm and laser energy at 150 mJ as previously presented by Arshad.A et al, 2021 (Ref 43). To cover the entire surface of coatings, the laser glazing was conducted with overlapped track was about 20% along straight lines. The samples were set on a motorized XY precision stage at room temperature, as shown in Fig. 1. Prior to performing the laser treatment, the energy was measured using a laser power and energy meter (Centauri, Ophir Optronics) for energy accuracy calibration.

Cyclic Oxidation Test

To evaluate the thermal cyclic behavior of the plasma-sprayed and laser-glazed TBC systems, a cyclic oxidation test was conducted in a high-temperature Carbolite Furnace (P330, Nabertherm, Germany) at 1000 °C. Each thermal cycle comprised of a 30-minute heating time at 1000 °C, followed by a 15-minute cooldown outside the furnace, and then returning the samples to the furnace for the next cycle. The spallation area of the coating was measured for both

Table 1 Specifications of materials used for various coating layers and the thickness of coating layers.

	Bond coat	Topcoat 1 (intermediate layer)	Topcoat 2 (top layer)
Material	NiCoCrAlYTa	ZrO_2-8 wt.% Y_2O_3	$La_2Zr_2O_7$
Coating thickness	150 ± 50 microns	250 ± 50 microns	80 ± 20 microns
Powder particle size range	5-38 microns	11-106 microns	53-106 microns

glazed and unglazed TBC systems after 100 cycles using ImageJ analysis. The thickness of the thermally grown oxide (TGO) versus cyclic oxidation time data was plotted to determine the TGO growth rate for both TBC systems.

Microstructural Characterization

The microstructural characterization of as-sprayed and as-glazed coatings was analyzed using field emission scanning electron microscopy (FESEM, Hitachi S-4160, Japan) and scanning electron microscopy (SEM, Hitachi SN3400, Japan) equipped with energy-dispersive x-ray spectrometer (EDS). Prior to SEM observation, the samples were prepared following standard metallographic techniques, and a gold layer was deposited on the samples by sputtering. Cross sections of the coating were examined under SEM, and images were collected for selected areas. Quantitative analysis of porosity level was performed on the polished cross section of the as-coated and as-glazed samples using image analysis software, ImageJ (provided by the National Institutes of Health, USA) in accordance with ASTM E2109-01 standard. TGO thickness was measured at 10-15 different locations on the polished cross-sectional SEM micrographs, and the average value was reported as TGO thickness.

Phase analysis was conducted using a x-ray diffractometry (XRD) (Smartlab, Rigaku, Japan) with Cu Kα radiation. The diffraction angle (2θ) range was between $2\mathring{0}$ and $8\mathring{0}$ at 40 kV. The average surface roughness (Ra) of

Table 2 HVOF spray process parameters for applying AMDRY 997 (NiCoCrAlYTa) bond coat (Ref 10)

Parameters	Value
O_2 flow rate	139 l/min
Propylene flow rate	89 l/min
Air flow rate	384 l/min
Feed rate	38 g/min
Distance	23 cm

Table 3 Atmospheric plasma spray process parameters for applying ZrO_2-8 wt.% Y_2O_3 and $La_2Zr_2O_7$

Parameters	ZrO_2-8 wt.% Y_2O_3(Ref 12)	$La_2Zr_2O_7$ (Ref 42)
Current, A	600	600
Voltage, V	70	70
Primary gas, Ar, l/min	38	35
Secondary gas, H_2, l/min	3	8
Powder feed rate, g/min	35	34
Spray distance, cm	12	10

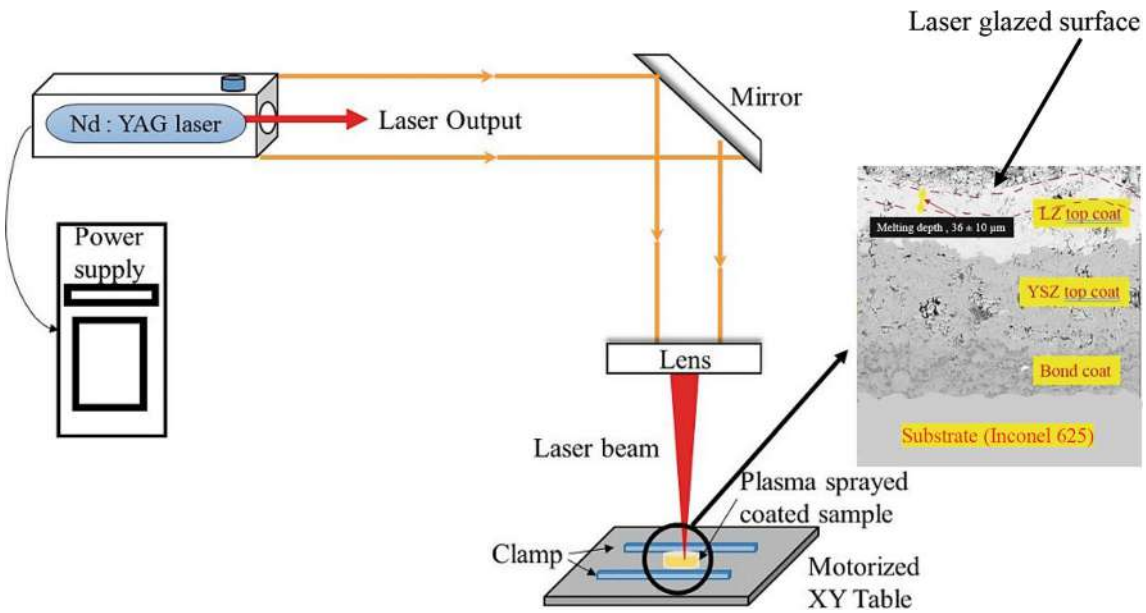

Fig. 1 Simplified schematic depiction of laser glazing system, modified from previous study (Ref 43). Reprinted from Materials Today: Proceedings, Vol. 39, Azrina Arshad, Muhamad Azizi Mat Yajid, Mohd Hasbullah Idris, Microstructural characterization of modified plasma spray LZ/YSZ thermal barrier coating by laser glazing, Pages 941-946, Copyright 2021, with permission from Elsevier

as-sprayed and laser-glazed coatings was measured using a roughness tester (SV2100, Mitutoyo, Japan), and the roughness value reported was the average of three values measured from different areas of the coating surface.

Results and Discussion

Characterization and Analysis of Coatings

The polished cross-sectional morphology of the as-sprayed and as-glazed LZ TBC coatings was observed through backscattered electron mode (BSE) scanning electron microscopy (SEM) images, as illustrated in Fig. 2. The sample's structure comprises three distinct layers: The LZ serves as the outermost layer, with YSZ positioned between the LZ and the metallic bond coat. Notably, YSZ exhibits a uniform thickness throughout. As depicted in Fig. 2(a), discernible defects in the form of pinholes and microcracks were evident on the uneven surface of the as-sprayed LZ coatings. This particular structure is a common characteristic of thermally sprayed coatings, primarily attributed to the inherent nature of the plasma spray process. It results in a lamellar microstructure intertwined with micro-defects. Notably, the as-sprayed LZ coatings displayed scattered voids within their cross section, which had an adverse impact on the coating's resistance to oxidation, as referenced in (Ref 44). These coatings possessed a porous microstructure, with an average porosity of approximately $15 \pm 0.1\%$, a value determined through ImageJ analysis. Following the laser glazing process, there was a noticeable reduction in pores and voids that had formed during the atmospheric plasma spray process in the top coat. The porosity experienced a slight decrease, measuring $8.9 \pm 0.24\%$, subsequent to the laser glazing procedure. As per Cernuschi's findings (Ref 45), porosity distribution in TBCs can be categorized into several classes, including dense (less than 10%), standard (10-15%), highly porous (15-20%), and very porous (greater than 20%). A higher degree of porosity in ceramic coatings ensures superior thermal insulation properties, resulting in lower thermal conductivity. However, it concurrently raises susceptibility to oxidation, corrosion, or accelerates chemical attack on the bond coat at elevated temperatures. The prevailing porosities within the sprayed coating are primarily a consequence of insufficient overlap between adjacent molten droplets and inadequate flattening during the plasma spray process.

Conversely, the presence of cracks in the coating arises from internal residual stress following plasma spraying, particularly during the cooling phase to ambient temperature (Ref 39). After the atmospheric plasma spray (APS) process, the rough surface of the LZ coating was found to have an average surface roughness (Ra) value of 7.07 ± 0.5 µm. Compared to the as-sprayed LZ coating, a dense top layer was obtained on the LZ coating surface after the laser glazing process, as depicted in Fig. 2(b). According to the literature, the most desirable characteristics of a laser-glazed layer are a 20-50 µm melting depth, non-segregation from the as-sprayed layer, a smoother

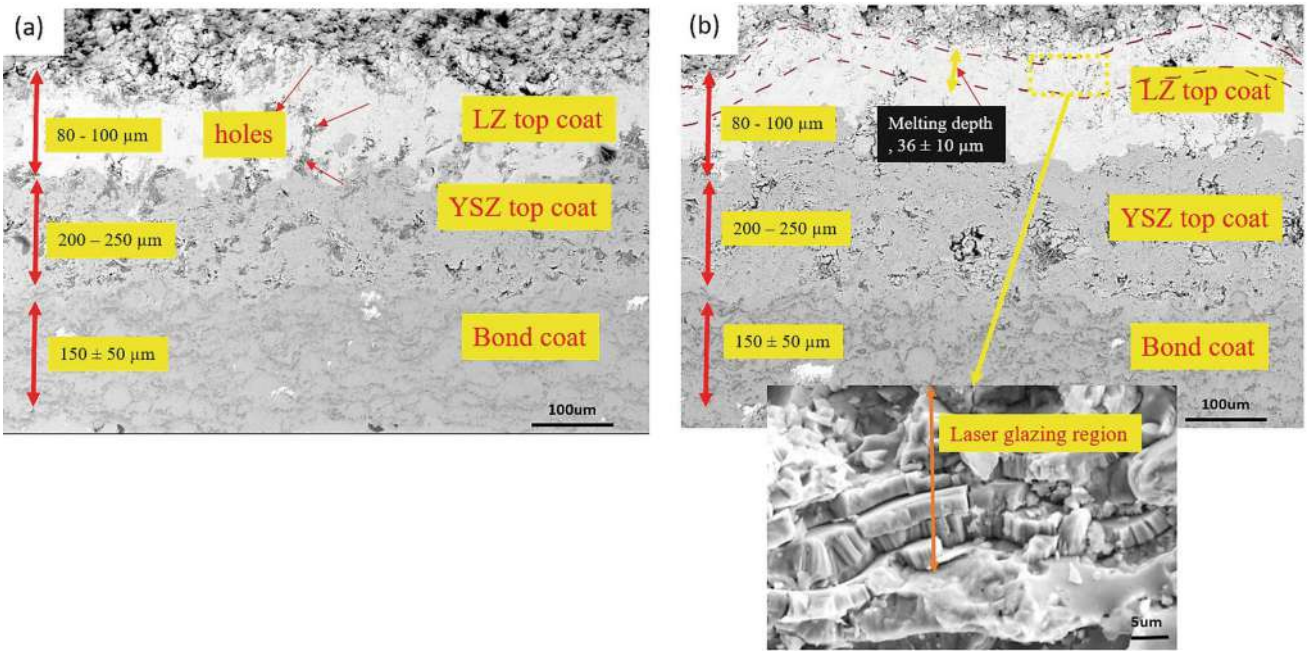

Fig. 2 Cross section morphology of (a) as-sprayed and (b) as-glazed LZ/YSZ TBC

surface with average surface roughness values (Ra) lower than 5 μm, and a distribution of the segmented cracks perpendicular to the surface (Ref 46-49). In this research, the accepted melting depth for the laser-glazed LZ top coat was obtained in the range of 36-46 μm, as shown in Fig. 2(b). The elongated type structure indicates that heat transfer occurs into the laser remelted plasma-sprayed region during rapid solidification. The surface roughness value of the glazed LZ coating was measured to be about 5.92 ± 0.5 μm. Laser glazing is an effective method for thermal barrier coating surface modification that involves remelting and rapid resolidification phenomena that reduce coating surface roughness (Ref 50, 51).

Figure 3 illustrates the surface morphology of both laser-glazed and as-sprayed LZ coatings. Fig. 3(a) exhibits distinct cracks that are oriented perpendicular to the surface. The aforementioned observation was ascribed to the phenomenon of shrinkage and thermal stresses that arise as a result of the rapid solidification occurring in the laser glazing process (Ref 5). There is speculation that the remelted layer undergoes a notable increase in density as a result of a substantial decrease in porosity following the laser glazing procedure. Due to the rapid cooling rate experienced by a molten pool, the laser-glazed TBC readily generates segmented cracks. As previously mentioned in other sources, the presence of segmented cracks serves a beneficial purpose by effectively accommodating the strain resulting from thermal cycles or the oxidation process of the metallic bond coat (Ref 4, 40, 52), as depicted in Fig. 3(b). The non-laser glazed or as-sprayed LZ/YSZ coating surface features a rough texture composed of fully melted splat structures, unmelted (or partially melted) particle regions, pores between splats, and cracks within the splats. The spraying circumstances have a significant effect on the microstructures of the coatings. The porosity of the coating is caused by inadequate overlap among the adjacent molten droplets and during flattening during the plasma spraying process, whereas the presence of cracks is caused by the internal residual stress created after the plasma spraying process (Ref 39).

XRD patterns of LZ ($La_2Zr_2O_7$) powder, as-sprayed and as-glazed double-layer thermal barrier coatings are shown in Fig. 4. The results indicate that the predominant phase of both as-sprayed and as-glazed LZ TBCs is $La_2Zr_2O_7$ (Ref 53) (JCPDS Card No. 01-074-8764). It is interesting to note that the higher diffraction intensity for as-glazed double-layer thermal barrier coating could be due to the preferred orientation of crystals in LZ TBC after laser-glazing (Ref 50).

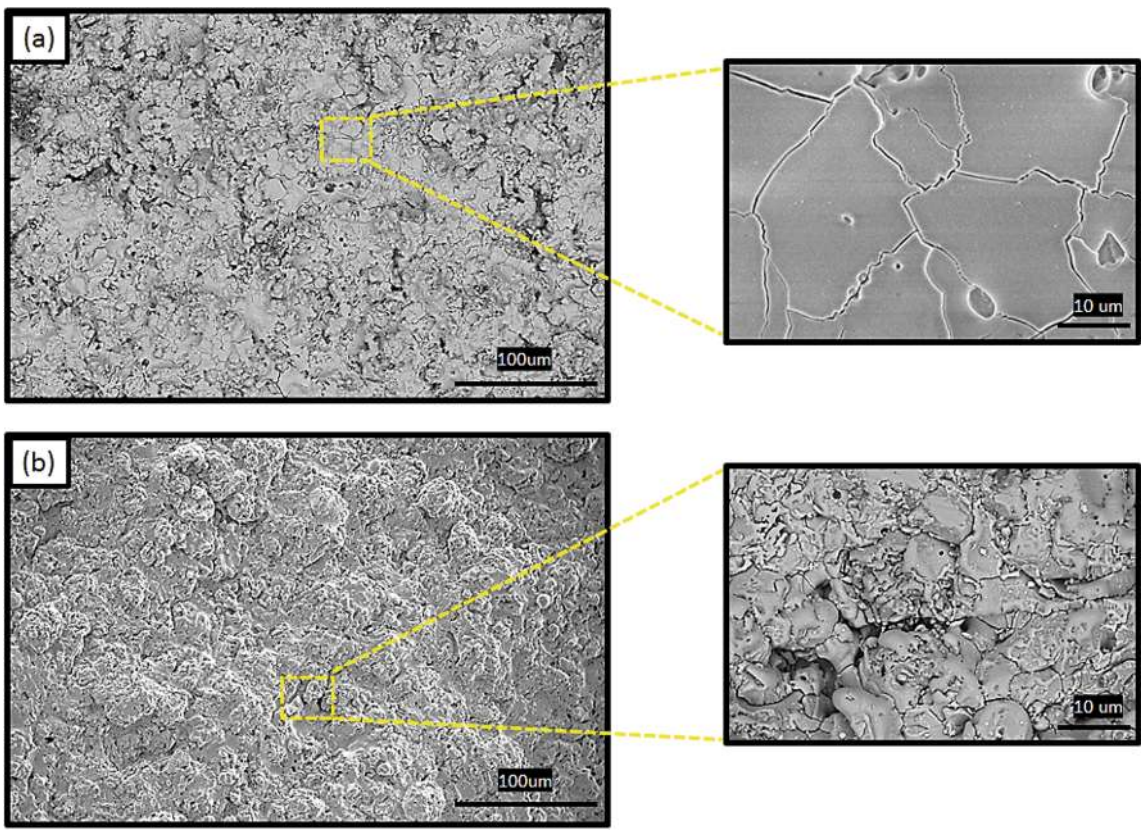

Fig. 3 Surface morphology of (a) as-laser glazed showing the segmented crack and (b) non-laser glazed showing the melted and unmelted zones

Characterization and Analysis of TBC Systems After Pre-Oxidation

Pre-oxidation in a argon-controlled environment with 99.995% Ar was carried out to establish a continuous, thin and slow growing TGO layer (mainly composed of α-Al_2O_3) at the interface between YSZ top coat and metallic bond coat before performing thermal cyclic tests (Ref 54). It was found that a continuous Al_2O_3 layer of TGO could be developed at the TC (ceramic top coat)/BC (metallic bond coat) interface under reduced oxygen pressure condition at high temperature (Ref 55).

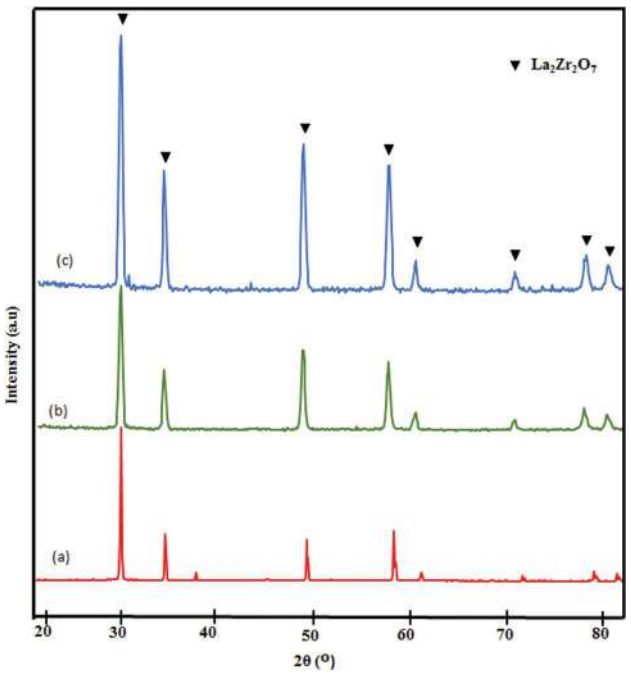

Fig. 4 X-ray diffraction analysis of (a) LZ ($La_2Zr_2O_7$) powder, (b) as-sprayed and (c) as-glazed double-layer thermal barrier coatings

Figure 5 shows the cross-sectional SEM images of APS TBC after pre-oxidation at 1000 °C for 12 h. In laser glazed sample, TGO shows the obvious formation of nearly continuous and thin Al_2O_3 layer (i.e., black layer of TGO) (Fig. 5b). However, as-sprayed coating (as shown in Fig. 5a) exhibits formation of discontinuous and non-uniform Al_2O_3 layer (i.e., black layer of TGO) along with noticeable formation of non-desirable mixed oxides (with fast growth) on top of the alumina layer during pre-oxidation treatment.

Figure 6(a) shows that the TGO layer is not uniform and may be made of mixed oxides instead of mostly alumina. This is supported in Fig. 6(c), which shows a lower weight percentage of Al. In contrast, it was easy to see a thin, continuous layer of Al_2O_3 at the interface between the bond coat and the YSZ layer in the as-glazed coating (Fig. 6b and d), which had a higher percentage of Al by weight. This Al_2O_3 layer is expected to act as a barrier against oxygen anion infiltration, effectively suppressing the growth of harmful oxides at the Al_2O_3/YSZ top coat interface during the thermal cyclic test at 1000 °C in as-glazed coatings. Figure 6(e) shows the EDS elemental mapping of the dense and continuous Al_2O_3 layer in as-glazed TBC coatings. The brighter layer of oxides above the Al_2O_3 layer likely consists of CS (Cr_2O_3- + Ni(Al,Cr)2O4, etc.), corresponding to a higher content of Cr at site A (in the non-laser glazed TBC system), which is 20.2 at.% compared to that of site B (as-glazed TBC system), where Cr content is 11.56 at.%. This suggests that mixed oxide clusters of chromia, spinel, and nickel oxide (CSN) are formed at the interface between the Al_2O_3 layer and topcoat. Laser glazing may modify the surface of the plasma sprayed coating, considerably reducing oxygen permeability into the TBC system at elevated temperature. In fact, the dense layer on top of the LZ coating could hinder oxygen transportation into the TBC system as well

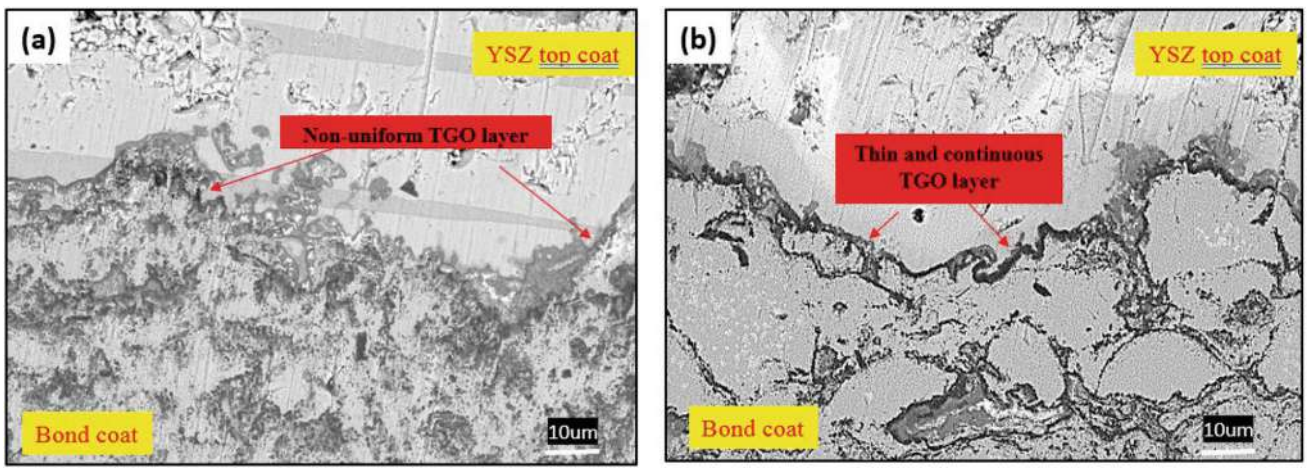

Fig. 5 SEM cross section microstructure after pre-oxidation test at 1000 °C for 12 hours (a) as-sprayed coating (b) as-glazed coating

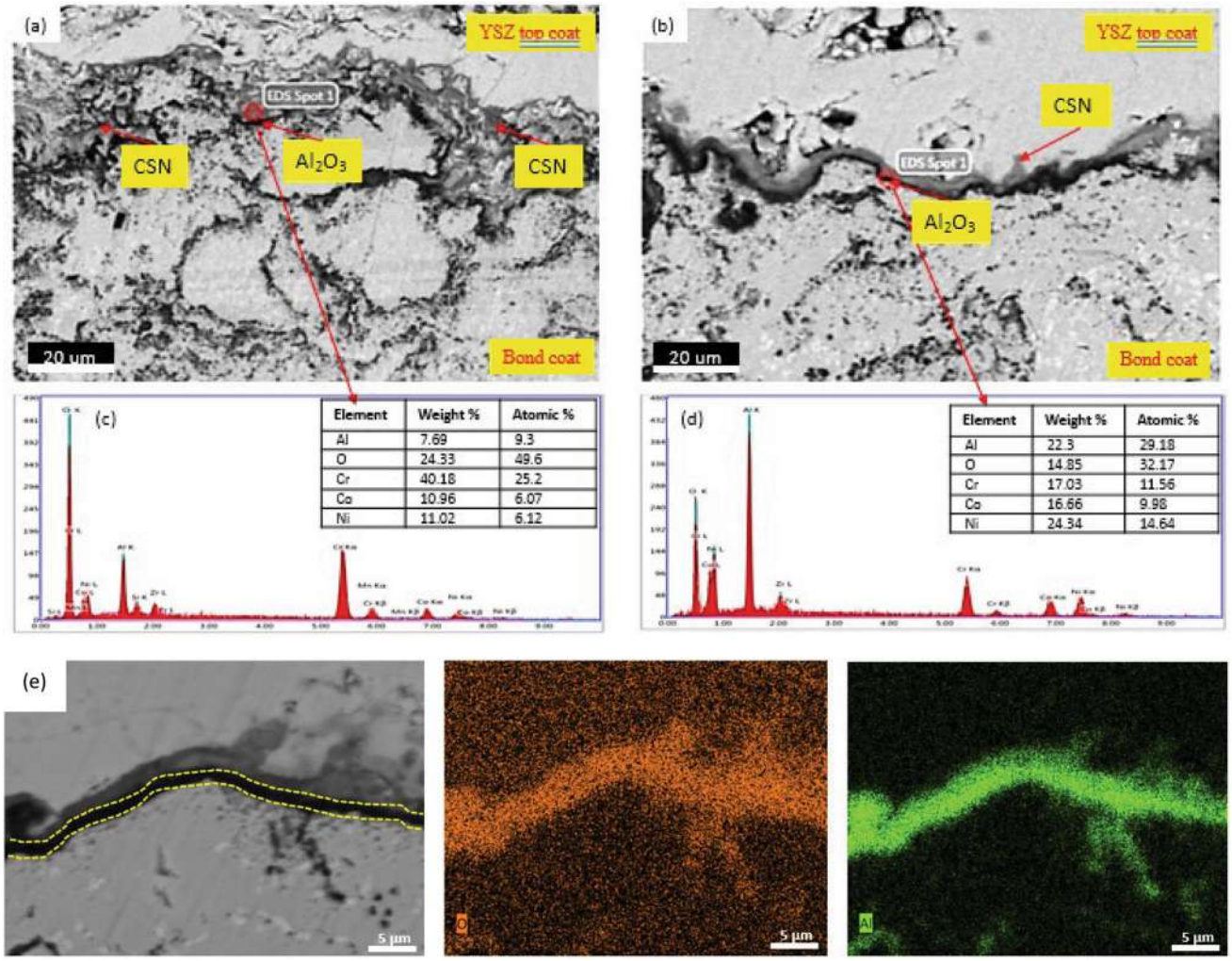

Fig. 6 The EDS analysis of pure TGO layer after pre-oxidation at 1000 °C. (a) and (c) for as-sprayed, (b) and (d) for as-glazed TBC coating and (e) elemental maps responding to dense layer for as-glazed

as the bond coat. In comparison with the non-laser glazed TBC system, the diffusion of O^{2-} was likely prevented in the early stage of the isothermal high-temperature pre-oxidation test in the laser-glazed TBC system, leading to the formation of the TGO layer mainly consisting of the Al_2O_3 layer.

Figure 7(a) and (b) shows the schematic illustration of non-laser glazed and laser glazed samples before and after pre-oxidation at 1000 °C for 12 hours. From Fig. 5 and 6, the observed thickness of the thermally grown oxide (TGO) layer in the non-laser glazed TBC system was noticed to be thicker than that of the laser glazed TBC system, mainly due to the higher porosity distribution in the TBC system with the non-laser glazed LZ top coat, as depicted in Fig. 7(a). In fact, the sealed surface of the LZ coating caused by the laser glazing process has been effective in withstanding the direct oxygen transportation during pre-oxidation in an argon-controlled environment, as shown in Fig. 7(b). Zhao et al. also noticed that the laser remelting process is able to considerably decrease the TGO thickness and growth rate because of the densified surface layer of the YSZ top coat, which reduces the oxygen diffusion rate during oxidation (Ref 56).

The dense uppermost layer of the laser-glazed LZ coating is expected to potentially delay the excessive growth of the thermally grown oxide (TGO), specifically the undesirable oxide growth on the alumina layer, when subjected to high-temperature thermal cyclic tests. The dense layer positioned above the laser-glazed LZ coating has the potential to impede the direct transport of oxygen toward the bond coat in the course of cyclic oxidation tests conducted in an air environment. It is noteworthy that the formation of Al_2O_3 at the interface of BC/TC, as indicated by its lowest Gibbs free energy of formation (G^0) compared to other oxides (Table 4), can be attributed to the high Al activity on the bond coat surface. This Al activity exhibits a

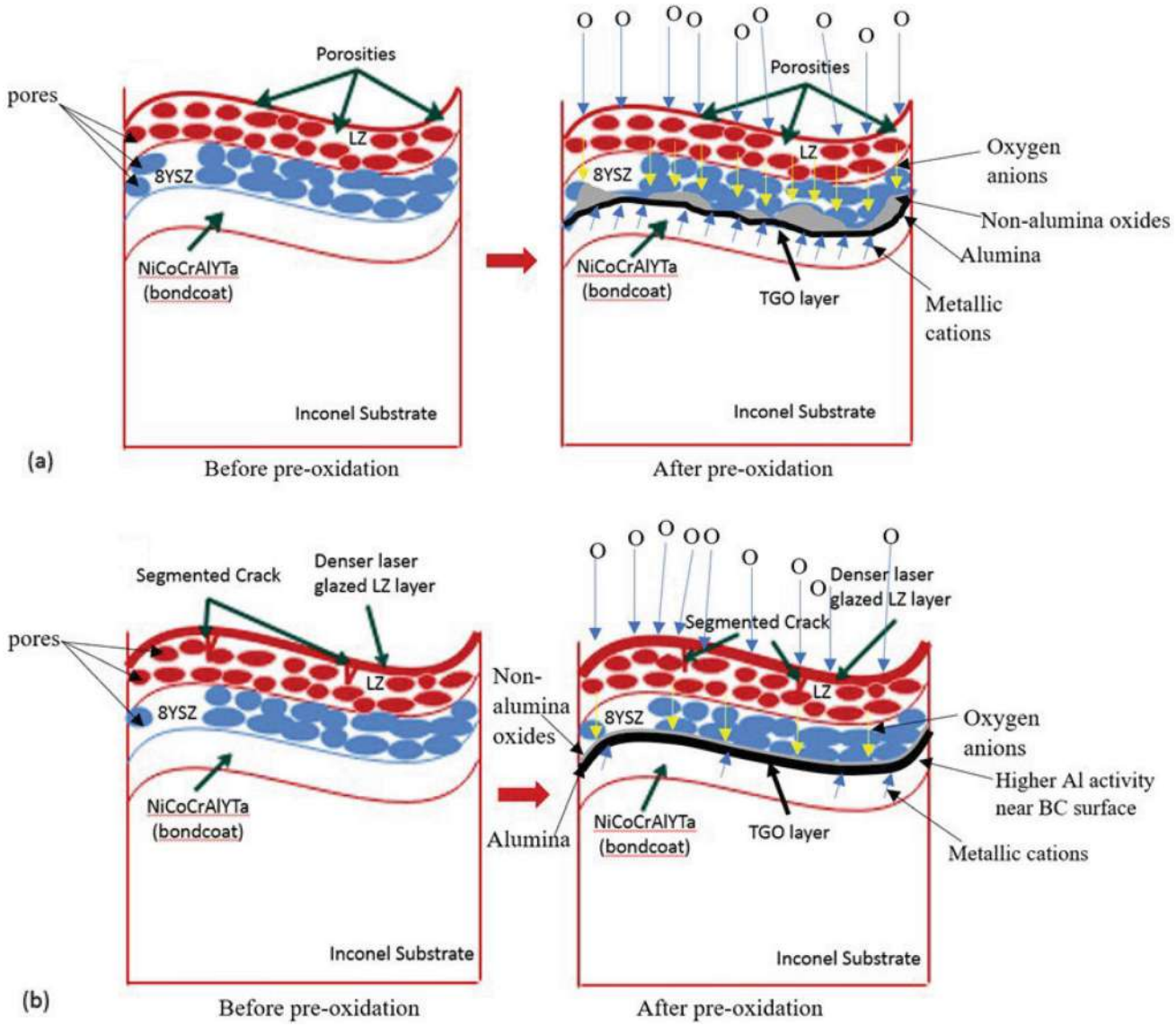

Fig. 7 Schematic illustration of the pre-oxidation behavior of TBCs at 1000 °C after 12 hours (a) non-laser glazed and (b) laser glazed samples

Table 4 Gibbs free energy of oxide formation, ΔG^0 (KJ/mole) at 1273 K (Ref 65, 69, 70)

Type of oxides	1273K, ΔG^0, KJ/mole
Al_2O_3	**− 850.5**
Cr_2O_3	− 520.7
NiO	− 256.9
CoO	− 343.4
$CoCr_2O_4$	− 101.5
$NiCr_2O_4$	− 42.9
$NiAl_2O_4$	− 115.4
$CoAl_2O_4$	− 93.3

strong affinity for reacting with O, leading to the outward penetration of Al cations and inward permeation of O anions (Ref 57). Furthermore, previous studies have indicated that the transportation of the reactants, such as cobalt (Co), nickel (Ni), chromium (Cr), and tantalum (Ta), across a continuous layer of alumina exhibits a significantly sluggish rate (Ref 58, 59). Similarly, it is anticipated that the presence of a thermally grown oxide (TGO) layer in a laser-glazed thermal barrier coating (TBC) system that has undergone pre-oxidation can lead to a reduced rate of TGO growth when subjected to thermal cyclic tests at a temperature of 1000 °C.

Comparison of Cyclic Oxidation Behavior of as-Sprayed and as-Glazed TBC Systems

Figure 8 shows pictures of the surface of the as-sprayed and as-glazed TBC systems after they were put through the thermal cycle tests. It can be seen that spallation of as-sprayed (Fig. 8a) and as-glazed (Fig. 8b) coatings was initiated from the edge of specimens, a relatively high-stress area. This is due to the faster temperature increment and decrease during thermal cycles at the edge compared to the other areas. This pattern of initial spallation has also been observed in other studies of the thermal cycles' effect on ceramics coatings (Ref 41). Early spallation started from the edge on the top coat (for the as-sprayed or non-laser-glazed TBC system) after 30 cycles, while the spallation didn't occur in the laser-glazed sample after 30 cycles. The edge spallation then propagated to the large area after the 50th and 80th cycles for as-sprayed samples (non-laser-glazed TBC system). The initial spallation in the as-glazed sample began after 80 cycles and gradually extended over 100 cycles. The spallation of about 20% of the coating area was discerned after 100 cycles for the as-sprayed (non-laser-glazed TBC system), while about 5% spallation of the coating area was detected for the as-glazed TBC system after 100 cycles, as shown in ImageJ analysis.

The extended lifetimes of as-glazed TBCs were believed to be due to a comparatively high segmented crack attributed to the top coat surface. Evidently, the network of segmented cracks formed by the laser glazing method resulted in a fourfold increase in thermal shock resistance, demonstrating the effectiveness of the laser glazing TBC system (Ref 40). Consequently, a pre-oxidized TGO layer in a laser-glazed TBC system may result in a slower rate of TGO growth at the bond coat/YSZ layer even during thermal cyclic tests.

On the other side, the large TGO thickness in the non-laser-glazed coating could be attributed to the fact that the non-laser-glazed coating is more transparent to oxygen compared to the laser glazed coating. Furthermore, micro-cracks will form and spread rapidly in TBCs during thermal cycles. This could be mitigated by the laser-glazed coatings. In fact, the open channels benefit from the thermal shock performance of the coating (in the laser-glazed TBC system) due to the enhanced strain tolerance (or strain adaptability improvement) (Ref 3). Segmented cracks produced by laser glazing improved the strain accommodation ability of the top coat and could be identified as the major enhancement mechanism for TBC lifetime extension (Ref 13).

The occurrence of micro-cracks, particularly the vertical through-thickness micro-cracks, in the non-laser-glazed

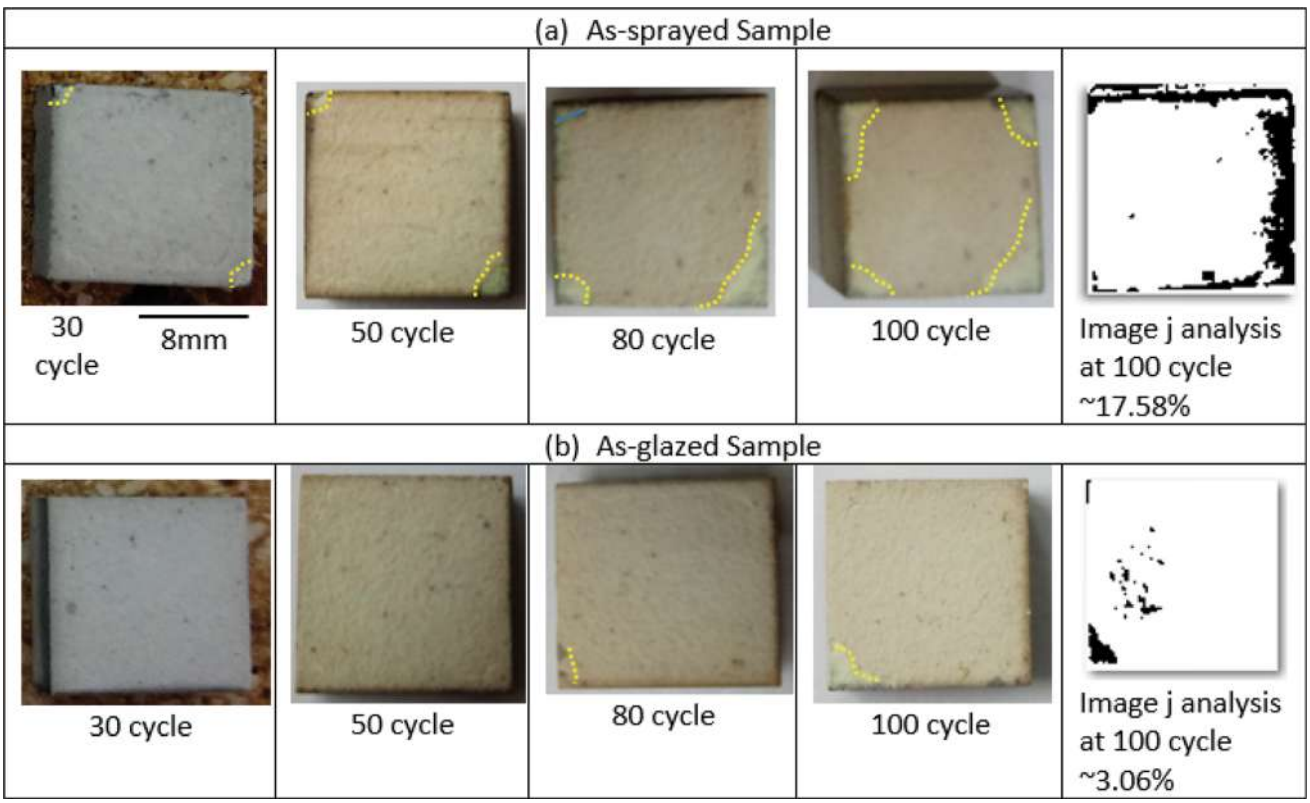

Fig. 8 Macroscopic image of :(a) plasma-sprayed and (b) laser-glazed samples during thermal cyclic test

coatings was found to result in an increase in the thermal conductivity of TBCs (Ref 7). This is further supported by the cross-sectional view shown in Fig. 9 for both laser-glazed and non-laser-glazed TBC systems, where distinct vertical micro-cracks are observed in the latter. These cracks are believed to serve as direct pathways for oxygen diffusion, leading to the accelerated growth of TGOs (as discussed in section 3.4) during thermal cyclic tests.

Figure 10 and 11 shows cross-sectional SEM images of the BC/TC interface of as-sprayed (Fig. 10a and b) and laser-glazed (Fig. 11a and b) TBC systems (TBCs) after the 30th and 80th cycles of the thermal cyclic test, respectively. The amount of Al and O elements was measured via EDS spot at A, B, and C points, as marked in Fig. 10 and 11(c and d) (performed on images with high magnification). Table 5 presents the EDS data at points A, B, and C

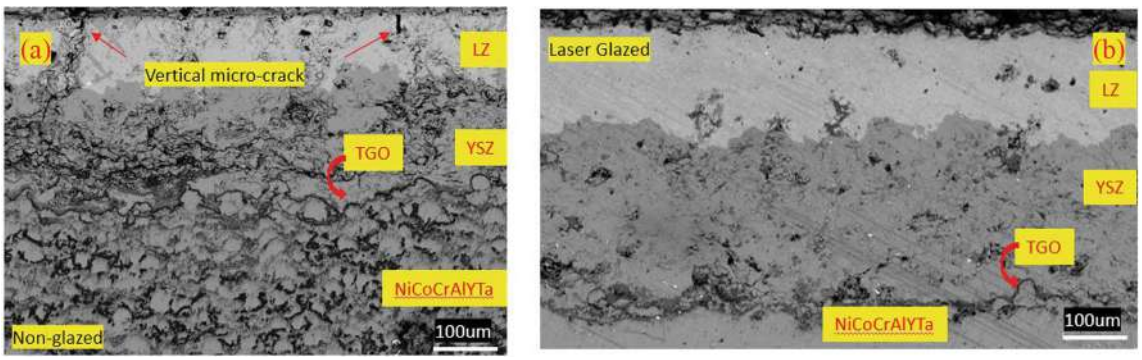

Fig. 9 Cross-sectional SEM image of (a) non-glazed (as-sprayed) and (b) glazed (as-glazed) TBC systems after 30th cycle of thermal cyclic test

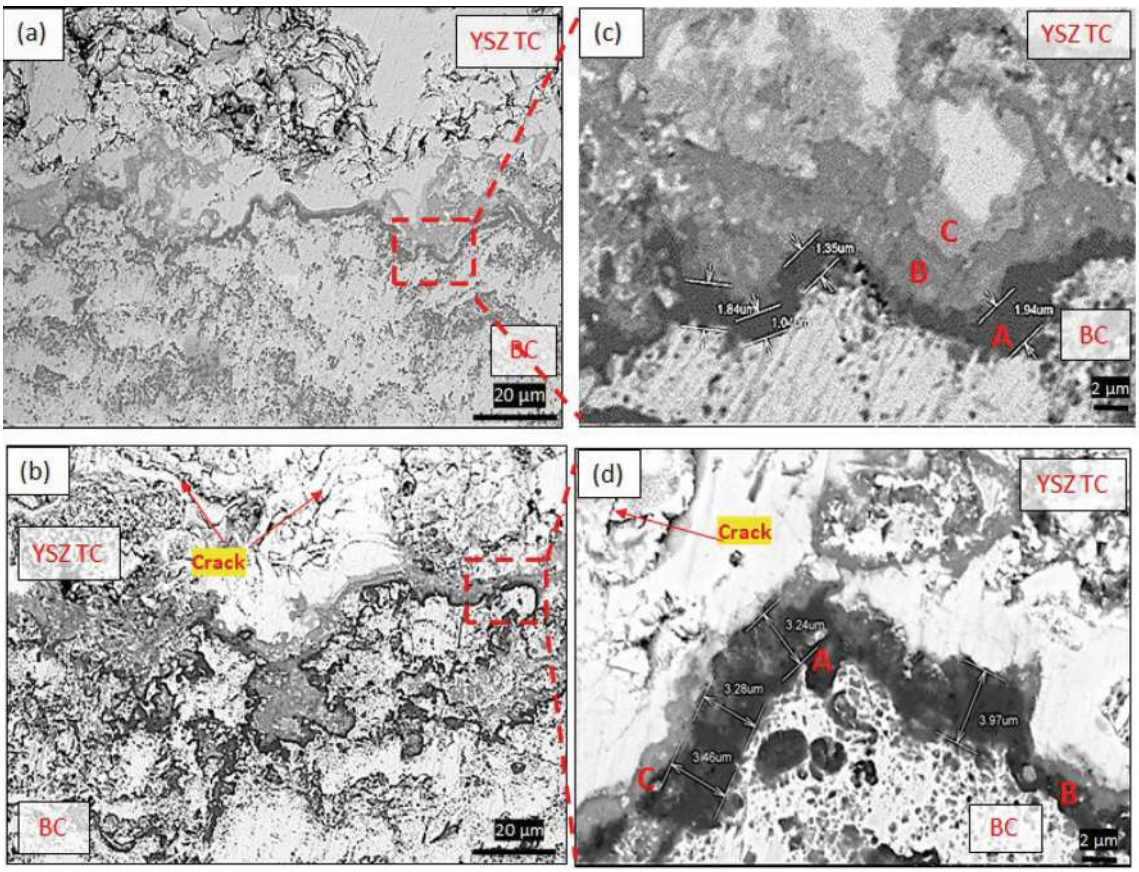

Fig. 10 Cross-sectional SEM images of BC/TC interface of as-sprayed sample after early thermal cycles at 1000 °C (a) after 30 cycles and (b) after 80 cycles. To clarify, high magnification images taken from red square areas in Figs. (a) and (b) were labeled as (c) and (d), respectively

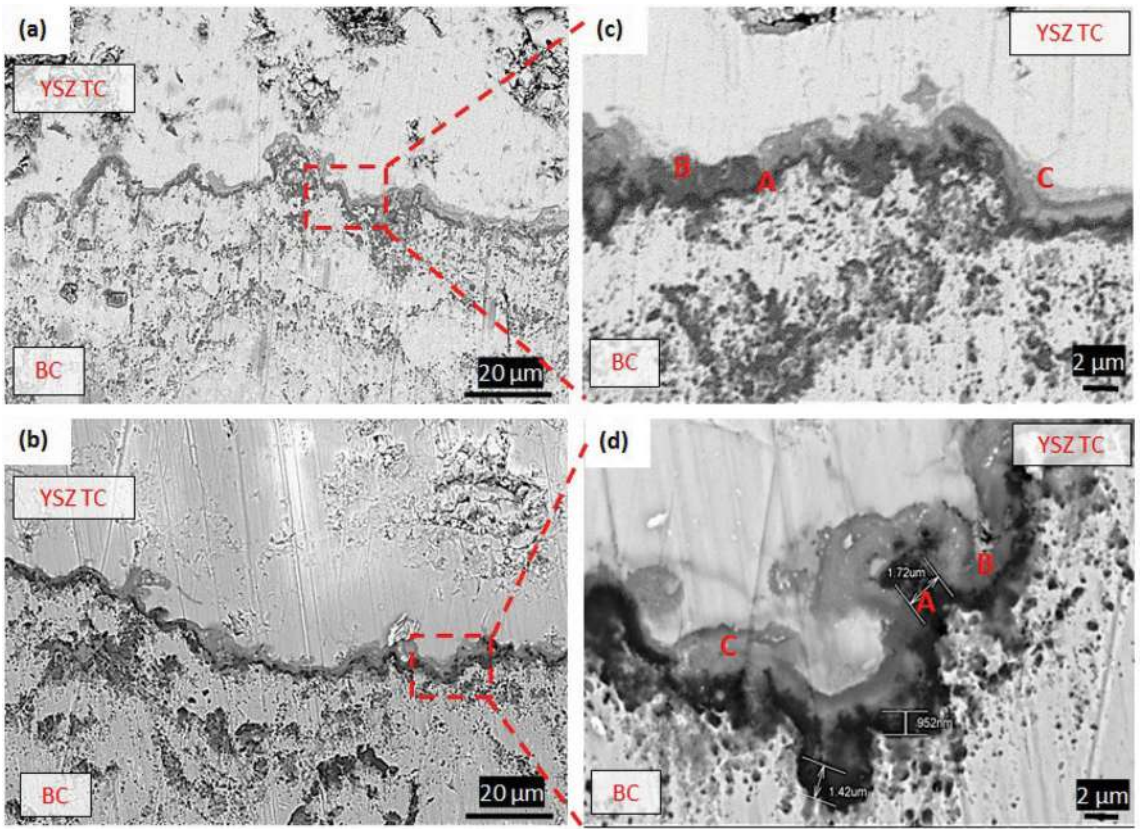

Fig. 11 Cross-sectional SEM images of BC/TC interface of laser-glazed sample after early thermal cycles at 1000 °C (a) after 30 cycles and (b) after 80 cycles. To clarify, high magnification images taken from red square areas in Figs. (a) and (b) were labeled as (c) and (d), respectively

Table 5 Elemental analysis at TC/BC interface of the TBC systems measured by EDS analysis

Point	Elements	As-sprayed		Laser-glazed	
		(at.%)	(wt.%)	(at.%)	(wt.%)
A	Al	24.62	28.21	34.35	40.01
	Co	6.93	7.43	9.93	8.32
	Cr	20.05	18.42	8.62	5.72
	Ni	13.93	8.32	10.72	12.03
	O	Bal.	Bal.	Bal.	Bal.
B	Al	10.36	12.43	14.15	20.23
	Co	12.61	20.23	19.02	28.21
	Cr	34	21.61	22.45	19.57
	Ni	11	15.19	30.95	25.63
	O	Bal.	Bal.	Bal.	Bal.
C	Al	20.66	16.20	20.84	14.33
	Co	14.69	10.12	14.87	8.07
	Cr	18.42	20.32	15.63	9.30
	Ni	10.58	8.53	10.86	18.32
	O	Bal.	Bal.	Bal.	Bal.

for both coating conditions, as referred to in Fig. 10(d) and 11(d) after 80 cycles. At point A, it looks like the dark layer of TGO is mainly composed of alumina (especially in the as-glazed sample). But according to EDS data at points B and C, the brighter layer of TGO could be caused by CSNs (non-desirable oxides) at the interface between the Al_2O_3 layer and the YSZ topcoat (Ref 57, 60). Mixed oxide clusters, or CSN clusters, can be made up of chromia, spinel, and nickel oxide. They are formed after Al_2O_3 because there aren't enough Al elements (or Al activity) near the surface of the bond coat (Ref 23). Previous research by Chen et al. (Ref 61) also supported this distribution of oxides. The contents of mixed oxides (CSNs) are larger in an as-sprayed TBC system than in a laser-glazed TBC system. The formation of harmful oxides during thermal exposure in the air would cause crack nucleation, resulting in premature TBC failure (Ref 23). This can significantly reduce the durability and lifetime of a TBC system. In other words, TGO layer formation and growth (particularly in the non-alumina oxide region), which are associated with the generation of stresses as well as a mismatch in the thermal expansion coefficient (TEC) between the TGO layer and the bond coat, can result in the formation of horizontal microcracks at the BC/TC interface

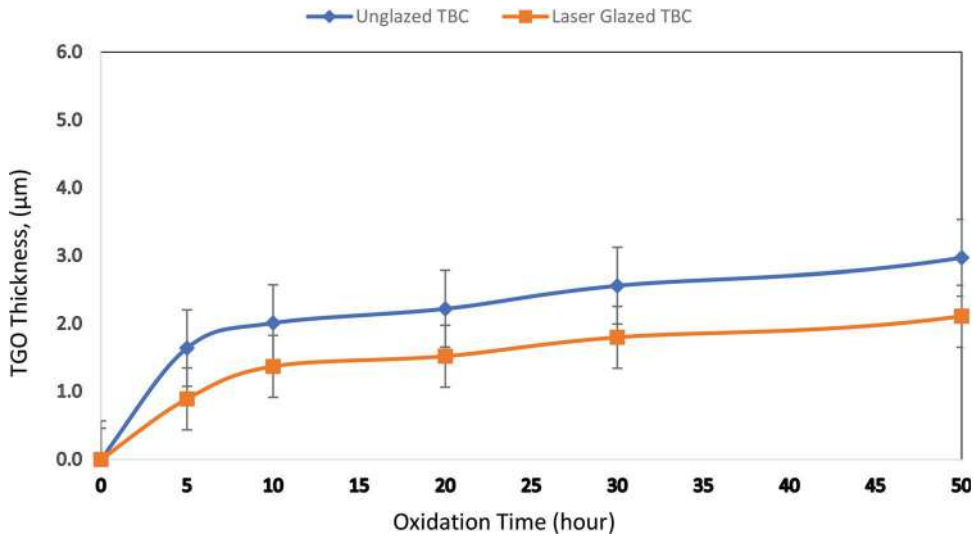

Fig. 12 The TGO thickness versus cyclic oxidation time

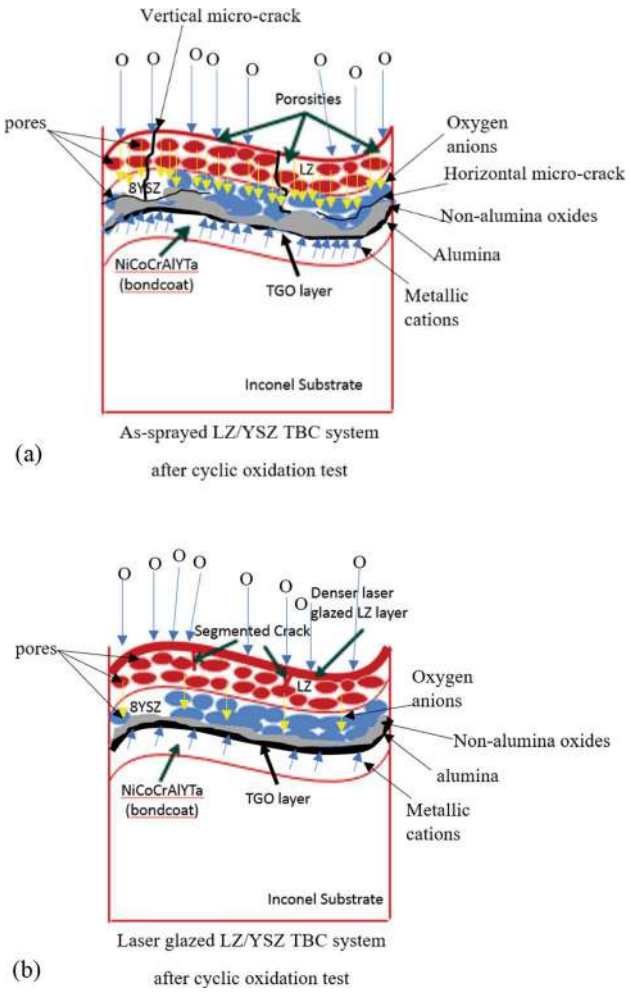

Fig. 13 Schematic illustration of the cyclic oxidation behavior of TBC systems at 1000 °C (a) as-sprayed or non-laser glazed and (b) laser-glazed TBC systems

(Fig. 9a). The formation of the TGO layer at the BC/TC interface can also be attributed to local expansion and stresses in the YSZ coating. This can result in horizontal microcracks and, eventually, the failure of the TBC coating (Ref 62).

Growth Kinetics of TGOs in TBC Systems During Thermal Cyclic Test and Related Mechanisms

TGO thickness was measured along the BC/TC interface in both the as-sprayed and laser-glazed TBC systems after different cyclic oxidation durations, as depicted in Fig. 12. Throughout the cyclic oxidation test, it is notable that the TGO thickness in the as-sprayed TBC system is considerably greater than that in the laser-glazed TBC system. This difference may be due to the sealed surface of the LZ coating within the TBC system, a result of the laser glazing process. This sealing effect can potentially limit oxygen ingress pathways, subsequently reducing the growth rate of TGO (Ref 63), even during thermal cycles (as indicated in Fig. 11). Moreover, the segmented cracks induced by the laser glazing process can effectively accommodate the thermal stresses arising from the coefficient of thermal expansion (CTE) mismatch between the ceramic top coat and the metallic bond coat (Ref 40, 41, 64). Additionally, it has been reported that the columnar grain microstructure observed in laser-glazed coatings allows for lateral expansion and contraction during heating and cooling processes, particularly during thermal cycles (Ref 5). These observed phenomena have the potential to influence the growth rate of TGO in the laser-glazed TBC system, primarily through the suppression of crack nucleation in both the top coat and the TGO layer.

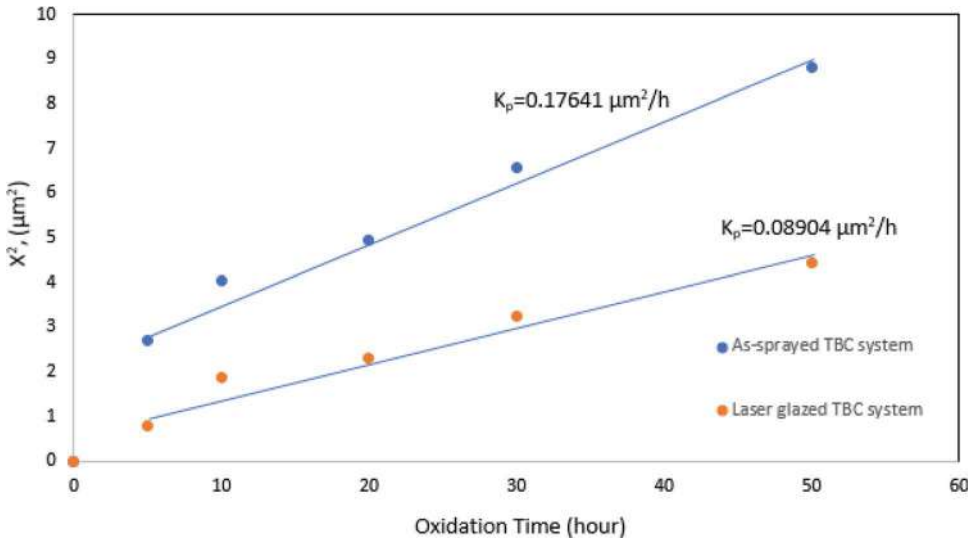

Fig. 14 Square of TGO thickness as a function of cyclic oxidation time

When the laser-glazed TBC system was compared to the as-sprayed TBC system, it appears that the TGO layer produced during the pre-oxidation process may have played a role in the lower TGO growth rate observed during the thermal cyclic test at 1000 °C. This is due to the TGO layer's continuous Al_2O_3 layer covering the bond coat surface, which acts as a diffusion barrier, slowing down the diffusion kinetics at a later stage of oxidation (Ref 65). As a result, the ability of other metallic cations in the bond coat to diffuse outward through the TGO (Al_2O_3 region) layer would be reduced. It is important to note that the lower TGO growth rate in the laser-glazed TBC system compared to the as-sprayed TBC system is due to this decrease in activity.

The inhomogeneous growth of complex mixed oxides was found to be responsible for the formation of higher tensile stresses at the outer layer of the TGO/YSZ interface. The growth stresses of α-Al_2O_3, $NiCr_2O_4$, NiO and CrO were reported to be 30.88, 62.99, 34.52 and 35.85 GPa, respectively (Ref 66). This indicates that the mixed oxides, particularly the spinel phase, are very perilous to the durability of the TBC, resulting in the formation of horizontal micro-cracks at that interface (Fig. 9a and 10b) (Ref 67). Thus, the propagation of those micro-cracks and cavities might lead to the providing easier diffusion pathways for the outward and inward of metallic cations and oxygen anions, respectively. This would significantly enhance the TGO growth rate and thickness during oxidation, similar to the as-sprayed TBC system compared to laser-glazed TBC system in this research (Fig. 12 and 13).

After the transient stage, the alteration of TGO thickness with time was noticed to follow the parabolic law. The kinetics TGO growth can be indicated through a following equation (Ref 26, 27):

$$X^n = K_p t \quad \text{(Eq 1)}$$

where x is considered as TGO layer thickness (µm), t is the time (h), the value of exponent (n) is regarded as 2 (assuming the growth mechanism is assisted by the diffusion process) and k_p is the growth rate constant. According to Fig. 12 and 14, the thickness and kinetics of the TGO layer are greater in the as-sprayed TBC system, which approximates parabolic behavior. The pattern obtained is similar to that previously studied by Cruchley et al (Ref 68).

Conclusion

The present study utilized the APS and HVOF processes to deposit LZ/YSZ ceramic top coats and NiCoCrAlYTa metallic bond coats on an Inconel 625 substrate. A pulsed Nd:YAG laser was employed to modify the surface of the plasma-sprayed LZ thermal barrier top coat. Both TBC systems were subsequently pre-oxidized at 1000 °C in an argon-controlled furnace. Thermal cyclic tests were conducted on the as-sprayed and laser-glazed TBC systems at 1000 °C for 30 minutes, followed by cooling outside the furnace for 15 minutes. The study yielded several significant findings, including:

1. Based on the observed TGOs at the BC/TC interface of TBC systems, the sealed surface of LZ coating (caused by the laser glazing process) was found to be able to withstand the direct oxygen transport during pre-oxidation in a high purity argon-controlled environment.
2. When compared to the as-sprayed TBC system, the TGO layer (produced during the pre-oxidation process) may have resulted in a lower TGO growth rate for the laser glazed TBC system.

3. It was discovered during the cyclic oxidation test that the TGO thickness in the as-sprayed TBC system is greater than that in the laser-glazed TBC system. This was due to the fact that the sealed surface of the TBC system's LZ coating (caused by the laser glazing process) could reduce oxygen ingress paths, thereby decreasing the growth rate of TGO in the laser-glazed TBC system during thermal cycles. Furthermore, the laser-induced segmented cracks can accommodate thermal stresses caused by the CTE mismatch between the ceramic top coat and the metallic bond coat.

Acknowledgment The authors would like to acknowledge Universiti Teknologi Malaysia (UTM) and Universiti Kuala Lumpur, Malaysian Institute of Industrial Technology (UniKL MITEC) for providing the research facilities and research grants, UTM Fundamental Research (UTM-FR Q.J130000.2551.20H66), UTM Transdisciplinary Grant—06G03 (UTM-TDR Q.J130000.3551.06G66) and UTM High Impact Research (UTM-HIR Q.J130000.2424.04G38).

References

1. R.J. Hunt, The History of the Industrial Gas Turbine (Part 1 The First Fifty Years 1940-1990), *Indep. Tech. Forum Power Gener.*, 2011, **582-2**, p 1-48.
2. A.D. Johari, A Review of Advance Thermal Barrier Coating Architecture, 2015, (April), p 8-9
3. C.S. Ramachandran, V. Balasubramanian and P.V. Ananthapadmanabhan, Thermal Cycling Behaviour of Plasma Sprayed Lanthanum Zirconate Based Coatings under Concurrent Infiltration by a Molten Glass Concoction, *Ceram. Int.*, 2013, **39**(2), p 1413–1431.
4. R. Ahmadi-Pidani, R. Shoja-Razavi, R. Mozafarinia and H. Jamali, Laser Surface Modification of Plasma Sprayed CYSZ Thermal Barrier Coatings, *Ceram. Int.*, 2013, **39**(3), p 2473–2480. https://doi.org/10.1016/j.ceramint.2012.09.005
5. R. Ghasemi, R. Shoja-Razavi, R. Mozafarinia and H. Jamali, The Influence of Laser Treatment on Thermal Shock Resistance of Plasma-Sprayed Nanostructured Yttria Stabilized Zirconia Thermal Barrier Coatings, *Ceram. Int.*, 2014, **40**(1), p 347–355. https://doi.org/10.1016/j.ceramint.2013.06.008
6. N.P. Padture, M. Gell, E.H. Jordan, P. Nitin and H. Eric, Thermal Barrier Coatings for Gas-Turbine Engine Applications, *Science*, 2002, **296**(5566), p 280–284. https://doi.org/10.1126/science.1068609
7. D.R. Clarke, M. Oechsner and N.P. Padture, Thermal-Barrier Coatings for More Efficient Gas-Turbine Engines, *MRS Bull.*, 2012, **37**(10), p 891–898.
8. M. Daroonparvar, M. Azizi, M.M.A.M. Yajid, N.M. Yusof, H.R. Bakhsheshi-Rad, Z. Valefi and E. Hamzah, Effect of Y_2O_3 Stabilized ZrO_2 Coating with Tri-Model Structure on Bi-Layered Thermally Grown Oxide Evolution in Nano Thermal Barrier Coating Systems at Elevated Temperatures, *J. Rare Earths, Chin. Soc. Rare Earths*, 2014, **32**(1), p 57–77. https://doi.org/10.1016/S1002-0721(14)60034-X
9. H. Yang, J. Zou, Q. Shi, M. Dai, S. Lin and W. Du, Analysis of the Microstructural Evolution and Interface Di Ff Usion Behavior of NiCoCrAlYTa Coating in High Temperature Oxidation, *Corros. Sci.*, 2019, **153**(Februry), p 162–169. https://doi.org/10.1016/j.corsci.2019.03.022
10. I.S.M. Zulkifli, M.A.M. Yajid, M.H. Idris, M.B. Uday, M. Daroonparvar, A. Emadzadeh and A. Arshad, Microstructural Evaluation and Thermal Oxidation Behaviors of YSZ/NiCoCrAlYTa Coatings Deposited by Different Thermal Techniques, *Ceram. Int.*, 2020, **46**(14), p 22438–22451.
11. J. Cao, K. Gao, X. Yu Cao and B. Jiang, Thermal Shock Behavior of a 8YSZ/CoCrAlYTaSi Thermal Sprayed Barrier Coating on GH202 Superalloy, *Ceram. Int.*, 2020, **46**(6), p 7489–7498.
12. M. Daroonparvar, M.A.M. Yajid, C.M. Kay, H. Bakhsheshi-Rad, R.K. Gupta, N.M. Yusof, H. Ghandvar, A. Arshad and I.S.M. Zulkifli, Effects of Al_2O_3 Diffusion Barrier Layer (Including Y-Containing Small Oxide Precipitates) and Nanostructured YSZ Top Coat on the Oxidation Behavior of HVOF NiCoCrAlTaY/APS YSZ Coatings at 1100 °C, *Corros. Sci.*, 2017, **2018**(144), p 13–34.
13. X.Q. Cao, R. Vassen, W. Jungen, S. Schwartz, F. Tietz and D. Stöver, Thermal Stability of Lanthanum Zirconate Plasma-Sprayed Coating, *J. Am. Ceram. Soc.*, 2004, **84**(9), p 2086–2090.
14. X.Q. Cao, R. Vassen and D. Stoever, Ceramic Materials for Thermal Barrier Coatings, *J. Eur. Ceram. Soc.*, 2004, **24**(1), p 1–10.
15. X.Q. Cao, R. Vassen, F. Tietz and D. Stoever, New Double-Ceramic-Layer Thermal Barrier Coatings Based on Zirconia-Rare Earth Composite Oxides, *J. Eur. Ceram. Soc.*, 2006, **26**(3), p 247–251.
16. E. Bakan and R. Vaßen, Ceramic Top Coats of Plasma-Sprayed Thermal Barrier Coatings: Materials, Processes, and Properties, *J. Therm. Spray Technol.*, 2017, **26**(6), p 992–1010.
17. Y. Zhang, M. Xie, F. Zhou, X. Cui, X. Lei, X. Song and S. An, Low Thermal Conductivity in La2Zr2O7 Pyrochlore with A-Site Partially Substituted with Equimolar Yb2O3 and Er2O3, *Ceram. Int.*, 2014, **40**(7), p 9151–9157. https://doi.org/10.1016/j.ceramint.2014.01.130
18. R. Vaßen, M.O. Jarligo, T. Steinke, D.E. Mack, D. Stöver, R. Vassen, M.O. Jarligo, T. Steinke, D.E. Mack, D. Stover, R. Vaßen and D. Stöver, Overview on Advanced Thermal Barrier Coatings, *Surf. Coat. Technol.*, 2010, **205**(4), p 938–942. https://doi.org/10.1016/j.surfcoat.2010.08.151
19. W.R. Chen, X. Wu, B.R. Marple and P.C. Patnaik, Oxidation and Crack Nucleation/Growth in an Air-Plasma-Sprayed Thermal Barrier Coating with NiCrAlY Bond Coat, *Surf. Coat. Technol.*, 2005, **197**(1), p 109–115.
20. W.R. Chen, X. Wu, B.R. Marple and P.C. Patnaik, The Growth and Influence of Thermally Grown Oxide in a Thermal Barrier Coating, *Surf. Coat. Technol.*, 2006, **201**(3–4), p 1074–1079.
21. M. Daroonparvar, Effects of Bond Coat and Top Coat (Including Nano Zones) Structures on Morphology and Type of Formed Transient Stage Oxides at Pre-Heat Treated Nano NiCrAlY / Nano ZrO 2-8 % Y_2O_3 Interface during Oxidation, *J. Rare Earths, Chin. Soc. Rare Earths*, 2015, **33**(9), p 983–994. https://doi.org/10.1016/S1002-0721(14)60516-0
22. M. Daroonparvar, M. Azizi Mat Yajid, N.M. Yusof and M. Sakhawat Hussain, Improved Thermally Grown Oxide Scale in Air Plasma Sprayed NiCrAlY/Nano-YSZ Coatings, *J. Nanomater.*, 2013, **2013**, p 1–9. https://doi.org/10.1155/2013/520104
23. A.G. Evans, D.R. Mumm, J.W. Hutchinson, G.H. Meier and F.S. Pettit, Mechanisms Controlling the Durability of Thermal Barrier Coatings, *Prog. Mater. Sci.*, 2001, **46**(5), p 505–553. https://doi.org/10.1016/S0079-6425(00)00020-7
24. M. Matsumoto, T. Kato, K. Hayakawa, N. Yamaguchi, S. Kitaoka and H. Matsubara, The Effect of Pre-Oxidation Atmosphere on the Durability of EB-PVD Thermal Barrier Coatings with CoNiCrAlY Bond Coats, *Surf. Coat. Technol.*, 2008, **202**(12), p 2743–2748.
25. L.Y. Lim and S.A. Meguid, Thermomechanical Simulations of the Transient Coupled Effect of Thermal Cycling and Oxidation

on Residual Stresses in Thermal Barrier Coatings, *Ceram. Int.*, 2022, **48**(3), p 3133–3147.
26. W.R. Chen, X. Wu, B.R. Marple, R.S. Lima and P.C. Patnaik, Pre-Oxidation and TGO Growth Behaviour of an Air-Plasma-Sprayed Thermal Barrier Coating, *Surf. Coat. Technol.*, 2008, **202**(16), p 3787–3796.
27. G. An, W. Li, L. Feng, B. Cheng, Z. Wang, Z. Li and Y. Zhang, Isothermal Oxidation and TGO Growth Behaviors of YAG/YSZ Double-Ceramic-Layer Thermal Barrier Coatings, *Ceram. Int.*, 2021 https://doi.org/10.1016/j.ceramint.2021.05.144
28. K.M. Doleker, Y. Ozgurluk and A.C. Karaoglanli, TGO Growth and Kinetic Study of Single and Double Layered TBC Systems, *Surf. Coat. Technol.*, 2021, **415**(March), p 127135. https://doi.org/10.1016/j.surfcoat.2021.127135
29. J. Toscano, R. Vaen, A. Gil, M. Subanovic, D. Naumenko, L. Singheiser and W.J. Quadakkers, Parameters Affecting TGO Growth and Adherence on MCrAlY-Bond Coats for TBC's, *Surf. Coat. Technol.*, 2006, **201**(7 SPEC. ISS.), p 3906–3910.
30. M. Nejati, M.R. Rahimipour and I. Mobasherpour, Evaluation of Hot Corrosion Behavior of CSZ, CSZ/Micro Al2O3 and CSZ/Nano Al2O3 Plasma Sprayed Thermal Barrier Coatings, *Ceram. Int.*, 2014, **40**(3), p 4579–4590. https://doi.org/10.1016/j.ceramint.2013.08.135
31. F. Zhou, Y. Wang, Z. Cui, J. Gou, Q. Zhang, C. Wang, L. Wang, J. Gou, Q. Zhang, C. Wang, L. Wang, J. Gou, Q. Zhang and C. Wang, Thermal Cycling Behavior of Nanostructured 8YSZ, SZ/8YSZ and 8CSZ/8YSZ Thermal Barrier Coatings Fabricated by Atmospheric Plasma Spraying, *Ceram. Int.*, 2016, **43**(October), p 0–1. https://doi.org/10.1016/j.ceramint.2016.12.014
32. H.X. Wu, Z. Ma, L. Liu, Y.B. Liu and D.Y. Wang, Thermal Cycling Behavior and Bonding Strength of Single-Ceramic-Layer Sm2Zr2O7 and Double-Ceramic-Layer Sm2Zr2O7/8YSZ Thermal Barrier Coatings Deposited by Atmospheric Plasma Spraying, *Ceram. Int.*, 2016, **42**, p 12922–12927. https://doi.org/10.1016/j.ceramint.2016.05.062
33. X. Wang, S. Guo, L. Zhao, Y. Zhu and L. Ai, A Novel Thermal Barrier Coating for High-Temperature Applications, *Ceram. Int.*, 2016, **42**, p 2648–2653.
34. Z. Liu, W. Zhang, J. Ouyang and Y. Zhou, Novel Double-Ceramic-Layer $(La_{0.8}Eu_{0.2})$2Zr2O7/YSZ Thermal Barrier Coatings Deposited by Plasma Spraying, *Ceram. Int.*, 2014, **40**(7), p 11277–11282. https://doi.org/10.1016/j.ceramint.2014.03.159
35. G. Di Girolamo, F. Marra, C. Blasi, M. Schioppa, G. Pulci, E. Serra and T. Valente, High-Temperature Mechanical Behavior of Plasma Sprayed Lanthanum Zirconate Coatings, *Ceram. Int.*, 2014, **40**(7 PART B), p 11433–11436.
36. M.G. Gok and G. Goller, Production and Characterisation of GZ / CYSZ Alternative Thermal Barrier Coatings with Multilayered and Functionally Graded Designs, *J. Eur. Ceram. Soc.*, 2016, **36**(7), p 1755–1764.
37. H. Zhou and D. Yi, Effect of Rare Earth Doping on Thermo-Physical Properties of Lanthanum Zirconate Ceramic for Thermal Barrier Coatings, *J. Rare Earths*, 2008, **26**, p 770–774.
38. M. Nejati, M.R. Rahimipour, I. Mobasherpour and A.H. Pakseresht, Microstructural Analysis and Thermal Shock Behavior of Plasma Sprayed Ceria-Stabilized Zirconia Thermal Barrier Coatings with Micro and Nano Al_2O_3 as a Third Layer, *Surf. Coat. Technol.*, 2015, **282**, p 129–138. https://doi.org/10.1016/j.surfcoat.2015.10.030
39. L. Wang, Y. Wang, X.G. Sun, J.Q. He, Z.Y. Pan and C.H. Wang, Thermal Shock Behavior of 8YSZ and Double-Ceramic-Layer La2Zr2O7/8YSZ Thermal Barrier Coatings Fabricated by Atmospheric Plasma Spraying, *Ceram. Int.*, 2012, **38**(5), p 3595–3606.
40. R. Ahmadi-Pidani, R. Shoja-Razavi, R. Mozafarinia and H. Jamali, Improving the Thermal Shock Resistance of Plasma Sprayed CYSZ Thermal Barrier Coatings by Laser Surface Modification, *Opt. Lasers Eng.*, 2012, **50**(5), p 780–786.
41. J.H. Lee, P.C. Tsai and C.L. Chang, Microstructure and Thermal Cyclic Performance of Laser-Glazed Plasma-Sprayed Ceria-Yttria-Stabilized Zirconia Thermal Barrier Coatings, *Surf. Coat. Technol.*, 2008, **202**(22–23), p 5607–5612. https://doi.org/10.1016/j.surfcoat.2008.06.118
42. G. Di Girolamo, F. Marra, M. Schioppa, C. Blasi, G. Pulci and T. Valente, Evolution of Microstructural and Mechanical Properties of Lanthanum Zirconate Thermal Barrier Coatings at High Temperature, *Surf. Coat. Technol.*, 2015, **268**, p 298–302. https://doi.org/10.1016/j.surfcoat.2014.07.067
43. A. Arshad, M.A.M. Yajid and M.H. Idris, Microstructural Characterization of Modified Plasma Spray LZ/YSZ Thermal Barrier Coating by Laser Glazing, *Mater. Today Proc.*, 2021, **39**, p 941–946. https://doi.org/10.1016/j.matpr.2020.04.145
44. S.Q. Xu, C. Zhu and Y. Zhang, Effects of Laser Remelting and Oxidation on NiCrAlY/8Y2O3-ZrO2 Thermal Barrier Coatings, *J. Therm. Spray Technol.*, 2018, **27**(3), p 412–422.
45. F. Cernuschi, Can TBC Porosity Be Estimated by Non-Destructive Infrared Techniques? A Theoretical and Experimental Analysis, *Surf. Coat. Technol.*, 2015, **272**, p 387–394. https://doi.org/10.1016/j.surfcoat.2015.03.036
46. M.G. Gok and G. Goller, Microstructural Evaluation of Laser Remelted Gadolinium Zirconate Thermal Barrier Coatings, *Surf. Coat. Technol.*, 2015, **276**, p 202–209. https://doi.org/10.1016/j.surfcoat.2015.06.074
47. G. Antou, G. Montavon, F. Hlawka, A. Cornet, C. Coddet and F. Machi, Modification of Ceramic Thermal Spray Deposit Microstructures Implementing in Situ Laser Remelting, *Surf. Coat. Technol.*, 2003, **172**(2–3), p 279–290.
48. H.L. Tsai and P.C. Tsai, Laser Glazing of Plasma-Sprayed Zirconia Coatings, *J. Mater. Eng. Perform.*, 1998, **7**(2), p 258–264.
49. R. Ghasemi, R. Shoja-Razavi, R. Mozafarinia, H. Jamali, M. Hajizadeh-Oghaz and R. Ahmadi-Pidani, The Influence of Laser Treatment on Hot Corrosion Behavior of Plasma-Sprayed Nanostructured Yttria Stabilized Zirconia Thermal Barrier Coatings, *J. Eur. Ceram. Soc.*, 2014, **34**(8), p 2013–2021. https://doi.org/10.1016/j.jeurceramsoc.2014.01.031
50. M.F. Morks, C.C. Berndt, Y. Durandet, M. Brandt and J. Wang, Microscopic Observation of Laser Glazed Yttria-Stabilized Zirconia Coatings, *Appl. Surf. Sci.*, 2010, **256**(21), p 6213–6218. https://doi.org/10.1016/j.apsusc.2010.03.143
51. C. Zhu, A. Javed, P. Li, F. Yang, G.Y. Liang and P. Xiao, A Study of the Microstructure and Oxidation Behavior of Alumina/Yttria-Stabilized Zirconia (Al2O3/YSZ) Thermal Barrier Coatings, *Surf. Coat. Technol.*, 2012, **212**, p 214–222.
52. J. Sure, A.R. Shankar and U.K. Mudali, Surface Modification of Plasma Sprayed Al2O3-40 Wt.% TiO2 Coatings by Pulsed Nd:YAG Laser Melting, *Opt. Laser Technol.*, 2013, **48**, p 366–374.
53. R. Wang, T. Dong, Y. Di, H. Wang, G. Li and L. Liu, High Temperature Oxidation Resistance and Thermal Growth Oxides Formation and Growth Mechanism of Double-Layer Thermal Barrier Coatings, *J. Alloys Compd.*, 2019, **798**, p 773–783. https://doi.org/10.1016/j.jallcom.2019.05.052
54. M. Daroonparvar, M.A.M. Yajid, N.M. Yusof, M.S. Hussain and H.R.B. Rad, Formation of a Dense and Continuous Al2O3 Layer in Nano Thermal Barrier Coating Systems for the Suppression of Spinel Growth on the Al2O3 Oxide Scale during Oxidation, *J. Alloys Compd.*, 2013, **571**, p 205–220.
55. W.R. Chen, X. Wu, D. Dudzinski and P.C. Patnaik, Modification of Oxide Layer in Plasma-Sprayed Thermal Barrier Coatings, *Surf. Coat. Technol.*, 2006, **200**(20–21), p 5863–5868.
56. C. Zhao, M. Zhao, M. Shahid, M. Wang and W. Pan, Restrained TGO Growth in YSZ/NiCrAlY Thermal Barrier Coatings by

Modified Laser Remelting, *Surf. Coat. Technol.*, 2017, **309**, p 1119–1125. https://doi.org/10.1016/j.surfcoat.2016.05.015
57. M. Saremi, A. Afrasiabi and A. Kobayashi, Microstructural Analysis of YSZ and YSZ/Al2O3 Plasma Sprayed Thermal Barrier Coatings after High Temperature Oxidation, *Surf. Coat. Technol.*, 2008, **202**(14), p 3233–3238.
58. L.C. Driver, HVOF Spraying of WC-Co & MCrAlY Coatings for Aeroengine Components. University of Nottingham, (2004)
59. Y. Tamarin, *Protective Coating for Turbine Blades*, ASM International, New York, 2002, p 247
60. L. Zhang, W. Fan, Y. Wang, K. Liu, Z.Z. Wang and Y. Bai, Oxidation Resistance of Plasma - Sprayed Double—Layered LC / YSZ Coatings with Different Thickness Ratios at High Temperatures, *Oxid. Met.*, 2020, **94**(0123456789), p 12.
61. W.R. Chen, X. Wu, B.R. Marple, D.R. Nagy and P.C. Patnaik, TGO Growth Behaviour in TBCs with APS and HVOF Bond Coats, *Surf. Coat. Technol.*, 2008, **202**(12), p 2677–2683.
62. M.S. Ahmadi, R. Shoja-Razavi, Z. Valefi and H. Jamali, The Effect of Laser Surface Treatment on the Thermal Shock Behavior of Plasma Sprayed Al2O3 /YSZ Multilayer Thermal Barrier Coatings, *Surf. Coat. Technol.*, 2019, **366**(January), p 62–69.
63. C. Zhu, P. Li, A. Javed, G.Y. Liang and P. Xiao, An Investigation on the Microstructure and Oxidation Behavior of Laser Remelted Air Plasma Sprayed Thermal Barrier Coatings, *Surf. Coat. Technol.*, 2012, **206**(18), p 3739–3746.
64. H. Chen, Y. Hao, H. Wang and W. Tang, Analysis of the Microstructure and Thermal Shock Resistance of Laser Glazed Nanostructured Zirconia TBCs, *J. Therm. Spray Technol.*, 2010, **19**(3), p 558–565.
65. S. Nath, I. Manna and J.D. Majumdar, Kinetics and Mechanism of Isothermal Oxidation of Compositionally Graded Yttria Stabilized Zirconia (YSZ) Based Thermal Barrier Coating, *Corros. Sci.*, 2014, **88**, p 10–22.
66. J. Shi, T. Zhang, B. Sun, B. Wang, X. Zhang and L. Song, Isothermal Oxidation and TGO Growth Behavior of NiCoCrAlY-YSZ Thermal Barrier Coatings on a Ni-Based Superalloy, *J. Alloys Compd.*, 2020, **844**, p 156093. https://doi.org/10.1016/j.jallcom.2020.156093
67. L.Y. Ni, C. Liu, H. Huang and C.G. Zhou, Thermal Cycling Behavior of Thermal Barrier Coatings with HVOF NiCrAlY Bond Coat, *J. Therm. Spray Technol.*, 2011, **20**(5), p 1133–1138. https://doi.org/10.1007/s11666-011-9647-8
68. S. Cruchley, H.E. Evans, M.P. Taylor, M.C. Hardy and S. Stekovic, Chromia Layer Growth on a Ni-Based Superalloy: Sub-Parabolic Kinetics and the Role of Titanium, *Corros. Sci.*, 2013, **75**, p 58–66. https://doi.org/10.1016/j.corsci.2013.05.016
69. S. Zhou, Z. Xiong, J. Lei, X. Dai, T. Zhang and C. Wang, Influence of Milling Time on the Microstructure Evolution and Oxidation Behavior of NiCrAlY Coatings by Laser Induction Hybrid Cladding, *Corros. Sci.*, 2016, **103**, p 105–116.
70. L. Zheng, M.C. Zhang, R. Chellali, H. Bouchikhaoui and J.X. Dong, Oxidation Property of Powder Metallurgy EP741NP Ni Based Superalloy at Elevated Temperatures, *Mater. Technol.*, 2013, **28**(3), p 122–128.